

Article

Cytotoxicity and UV Light Absorption in Biopolymeric Membranes from Native Vegetation of Mexico

Mayela Alhelí García de Alva Magos ^{1,2}, Jesús Santa-Olalla Tapia ³,
Miguel Ángel Ramos López ⁴, Jessica Molina Maturano ², Antonio Ruperto Jiménez Aparicio ¹,
Brenda Hildeliza Camacho Díaz ¹ and Luz Arcelia García Serrano ^{2,*}

¹ Centro de desarrollo de Productos Bióticos (CEPROBI) del Instituto Politécnico Nacional, Carretera Yautepec-Jojutla, Km 6, calle CEPROBI No. 8, Col. San Isidro, Yautepec C.P. 62731, Mexico; mgarciadealvam1600@alumno.ipn.mx (M.A.G.d.A.M.); aaparici@ipn.mx (A.R.J.A.); bcamacho@ipn.mx (B.H.C.D.)

² Centro Interdisciplinario de Investigaciones y Estudios sobre Medio Ambiente y Desarrollo (CIEMAD) del Instituto Politécnico Nacional, Calle 30 de Junio de 1520 s/n, Barrio Laguna Ticomán, Alcaldía Gustavo A. Madero, Ciudad de México C.P. 07340, Mexico; jmolinam1600@alumno.ipn.mx

³ Facultad de Medicina, Universidad Autónoma del Estado de Morelos (UAEM), Calle Leñeros esquina Iztaccíhuatl s/n Col. Volcanes, Cuernavaca C.P. 62350, Mexico; jsa@uaem.mx

⁴ Facultad de Química, Universidad Autónoma de Querétaro (UAQ), Centro Universitario, Cerro de las Campanas s/n, Cto Universitario, Santiago de Querétaro C.P. 76010, Mexico; miguel.angel.ramos@uaq.mx

* Correspondence: lugarcias@ipn.mx or draluzg81ds@gmail.com

Received: 26 May 2020; Accepted: 8 July 2020; Published: 21 July 2020



Abstract: Sustainable processing from native vegetation such as agave, nopal and aloe, is mainly centered on the components of lignin, cellulose, and hemicellulose, defined generally as lignocellulosic. Cytotoxicity of lignocellulosic biopolymer membranes (LBMs) of mucilages of *Opuntia ficus-indica*, *Aloe barbadensis* Miller, fructans, and residual *Agave tequilana* Weber fibers at different concentrations (30, 50 and 70%), was evaluated in contact with human fibroblast cells (ATCC[®] PCS-201-010), cultured in vitro. Long and short LBMs were formed from the fibrous material. The interaction showed mild cytotoxicity according to ISO 10993-5: 2009. Cytotoxic activity demonstrated in the presence of fibroblasts implied a maximum cytotoxicity of close to 46% and a minimum of 7% in LBMs. UV light absorption results of the large fiber LBMs showed the highest prevention of passage of light, having a protective effect mechanism of delaying the response of hypersensitivity as a result of exposure to UV radiation. The morphology and structure were characterized using SEM, FT-IR, and image texture analysis. According to the LBMs reactivity measured, the feasible uses of these membranes can be suggested as materials for biomedical applications over a short period of time, with feasibility as a support to provide some beneficial solutions.

Keywords: endemic plants; lignocellulosic; biopolymers; cytotoxicity; fibroblasts; UV

1. Introduction

Native vegetation is all plant species that materialize naturally in a particular habitat and provide essential habitat. These plants have evolved through time adapting to the soil, temperature, nutrients, and weather of their region, being naturally resilient because these are adapted to local conditions. A characteristic native vegetation of Mexico is the agave plant. However, Agavaceas in Mexico are characterized by the large-scale generation of residuals from alcoholic beverage production processes. Due to this, it is of great interest to re-use the subproducts. For each ton of bagasse of *Agave tequilana* Weber, 3.1% of fiber is obtained. In addition to this, *Opuntia ficus-indica* and *Aloe barbadensis* Miller, are both species from Mexico [1,2]. The *Agave tequilana* Weber fibers are mainly composed of cellulose

(43%), hemicellulose (19%), lignin (15%), and sugars (10%), among others [3]. Therefore, they are called lignocellulosic materials.

These types of biomaterials have been promoters of exponential growth in the last five decades and there is a rising trend [4]. These materials can imitate the properties of natural tissue, fulfilling the requirements of functional feasibility, biostability, biocompatibility, and sterility, among others [5]. These requirements could guarantee applications of these residuals as new materials with a new application.

Biodegradable polymeric biomaterials have two main advantages. First, they do not cause permanent chronic reactions to foreign bodies since they are gradually absorbed by the human body and do not leave permanent traces of residues in the tissues where they are implanted. Secondly, it has been found recently that some of them can integrate cells into their structure, which allows devices to be generated in the most conducive ways for the restoration of function [6]. Therefore, many starch derivatives, cellulose esters, such as acetate, nitrocellulose, and cellulose derivatives [7] are being considered as a good option to restore the manufacture of membranes and hollow fibers suitable for enzyme immobilization and applications as matrices for drug delivery and as wound dressings [8].

Natural materials often exhibit different structural characteristics according to the size of the particles, which establishes diversity in their porosity; on the other hand, depending on the source, it is possible to have fibrous structures at different scales [9]. Some applications of composite materials in biomaterial applications are joint replacements, bone plates, bone cement, ligaments, artificial tendons, dental implants, heart valves, blood vessels, skin repair, and protection devices [4].

The skin is considered the largest organ in most vertebrate organisms, having a complex structure (the epidermis, the dermis, and the hypodermis), which under normal conditions can self-regenerate. Considering that disorders, trauma, chronic wounds, and burns can occur sometimes, which can result in extensive and deep wounds, disturbing the anatomical and physiological structure of the tissue and representing considerable damage to the natural defense barriers with foreign agents [10], the current approach to biomaterial engineering for the medical treatment of skin lesions has focused on the possibility of replacing damaged tissue using live cells in combination with different biomaterials used as scaffolding or support for regeneration of injured tissue [11]. Wound healing is a natural process of the body and an appropriate dressing may be able to improve the healing process considerably, providing suitable conditions for healing [12].

More and more evidence indicates that the use of sunscreen is not completely safe for skin protection. Since epidemiological studies indicate that an incorrect application carries a history of skin cancer [13]. Natural materials have been considered as potential sun protection resources due to their absorption of UV radiation in addition to antioxidant activity [14]. Therefore, natural agavaceous biopolymers could be important sources for the investigation of new biocompatible compounds. It is necessary to focus on new biological mechanisms in order to obtain new active molecules and study the relationship between structure and function to develop more active medical devices in addition to avoiding unwanted side effects such as sensitivity to the sun or the inaccuracy of the application [15].

Although UV radiation has some benefits, its negative effect on human health is much greater. Skin cancer is one of the most documented consequences [16].

Cellular and tissue response are key factors in the design and application of successful biomaterials. One method to evaluate the cellular and tissue response is to measure cytotoxicity *in vitro*, or its quality of being toxic to a cell. Cellular toxicity (death) is determined by the survival (viability) of a population before exposure of the compound or inhibition of cell proliferation [17]. Cell viability assays are used as routine tests to study the impact that a given compound could have on cell proliferation, as well as the direct cytotoxic effects that eventually lead to cell death. Cytotoxicity provides the initial information required for us to address any other type of tissue response [18].

The molecular mechanisms of cellular toxicity allow determining the main substances and functional groups with cytotoxic capacity. This favors the identification of the most sensitive cell types [19]. Therefore, the widespread use of polymers requires that the potential interaction of biomaterials with cells, in this case fibroblasts, be known. Since specific diploid human fibroblasts

are a specific model for the early recognition of possible cytotoxic effects of potential materials for the development of biocompatible components [20], these were used for cytotoxicity testing and information regarding any potential uncertainties with the tissue response [21]. For cytotoxicity tests ISO 10993-5: 2009 was developed, around the evaluation of materials and devices, regarding their usefulness as biocompatible materials. [22].

There is previous research in the use of natural fibers used as materials for the formation of biopolymeric materials. In a study conducted in Brazil, sisal and coconut fibers with an added emulsion were used as a matrix to produce composite soil. The results of the tests demonstrated that water absorption of sisal fibers is much greater than coconut fibers, depending on the orientation of the fibers within the matrix and their microstructure [23].

In other investigations, polymer compounds reinforced with natural fibers (bamboo, sisal, jute, etc.) have been obtained. These compounds have beneficial properties such as low density and less cost and solidity compared to synthetic compounds, which provides advantages for their use in commercial applications (automotive, buildings, and construction). The use of natural fibers as reinforcement for polymeric compounds introduces a positive effect in the mechanical behavior of polymers. Mohammed et al., 2015 evaluated the properties: mechanical, thermal, energy and moisture absorption. As well as the viscoelastic behaviors, degree of biodegradability of the fibers of the polymeric compounds reinforced with natural fibers by adding coupling agents [24].

In the case of cellulosic substrates, biocomposites were developed in two proportions of hyaluronic acid and cellulose, which showed a variety of morphological and structural changes, as well as biocompatibility results, suggesting their beneficial application in wound care devices [25]. On the other hand, researchers evaluated cellulose compounds in epithelial regeneration focusing on modifications such as topography, water content, and pore structure in combination with other polymers and found applications and positive effects in dermal applications [26].

This work consisted of performing the development and characterization of a method to re-use material manufactured from agave fiber and natural binders in order to provide the sustenance for a possible application of the membranes as support and use in skin care by carrying out a preliminary evaluation of the degree of cytotoxicity. Furthermore, the UV light absorption behavior and other properties such as Scanning Electron Microscope (SEM), stereoscopic microscopy, Fourier transform infrared spectroscopy (FT-IR), and image analysis were determined. The main advantages of this approach are the ease of fabrication, as cross-linking agents come from native vegetation. The preparation of these membranes demonstrates a promising alternative as a dressing material.

2. Materials and Methods

2.1. Agaveaceous Materials for the Conformation of the Membranes

2.1.1. Obtaining Fibrous Material

The fibrous material contained in the stem (32.9 brix degrees) was extracted by cutting from the seven-year-old crop of *Agave tequilana* Weber in the Laboratory of Permaculture and Eco design of Nano-microfibers, with coordinates 19°30'52.7" N, 99°07'45.2" W, in Mexico City. It underwent a crushing machine process with slow kinetics by passing through mechanical rippers at a temperature of 80 °C and a constant pressure of 300 MPa for 6 h. It was then washed with water at room temperature until the last wash was neutral (no sugars).

This was dried in a tray dryer at a temperature of 60 °C for 24 h until a relative humidity content of 5% was obtained. Half of the dry product was milled in a mechanical Pulvex® (mill of grains) blade mill until the size of the fibers was reduced to between 1 and 4 cm in length, which are called long fibers (FL). The other half were subjected to a further grinding, passing the fiber through a sieve (N. 150) until a particle size between 10 and 15 µm was obtained. They were then heated on stove at 37 °C for 24 h until a relative humidity content of 5% was obtained, and they are named curt fibers (FC).

2.1.2. Obtaining *Opuntia ficus-indica* Mucilage

Vegetative material from the five-year harvest of *Opuntia ficus-indica* from the laboratory of permaculture and eco design of nano microfibers, with coordinates 19°30'52.7" N, 99°07'45.2" W, in Mexico City was used. Cladodes were selected, homogeneous in size (between 40 and 55 cm in length) and age. The spines were removed, cut into pieces, and then crushed in an industrial blender and homogenized in aqueous medium at a 1:5 ratio in a mixer with rotating blades for 3 min. The mixture was subjected to a heating process for 20 min at 85 °C at approximately 3500 rpm (pH 4–4.5). This mixture was filtered through an N.150 sieve to later be centrifuged (Beckman, Avanti J-25) at 4000 rpm for 15 min.

2.1.3. Obtaining *Aloe barbadensis* Miller Mucilage

Vegetative material from a three-year crop of *Aloe barbadensis* Miller from the laboratory of permaculture and eco design of nano microfibers, with coordinates 19°30'52.7" N, 99°07'45.2" W, in Mexico City was used. Leaves were selected and sliced homogeneously (between 30 and 45 cm).

The dowels, which are along its edges, were removed before cutting the leaves. The leaves were washed with distilled water to remove dirt from the environment. The epidermis was carefully separated from the parenchyma using a scalpel. This pulp was washed with distilled water and then it was crushed in an industrial blender and homogenized in aqueous medium at a ratio of 1:5 in a mixer with rotating blades for 3 min. The mixture was subjected to a heating process for 20 min at 85 °C at approximately 3500 rpm (pH 4–4.5). This mixture was filtered through an N.150 sieve to later be centrifuged (Beckman, Avanti J-25) at 4000 rpm for 15 min.

2.1.4. Obtaining Fructans

Agave fructans were extracted using a pilot modular system for the extraction of agave fructans (Patent No. MX/E/2015/087857, "Modular system and process to obtain several products from agave fructans") designed by CeProBi researchers. Through this system, a liquid extract with a high content of fructans was obtained, which was subsequently dehydrated by spray drying, with a rotary disk dryer, whose inlet and outlet temperature was 200 and 70 °C, respectively, for 24 h, until the moisture content was 5%.

2.2. Obtaining Lignocellulosic Biopolymer Membranes

Lignocellulosic biopolymer membranes (LBMs) were prepared with different compositions of the fibrous material. To define the concentrations of the fibrous material, a sweep from 5 to 90% of the concentration was performed in the UV radiation absorption processes, defining significant differences at 30, 50 and 70% of fibrous material at the different wavelengths.

For the conformation of the LBMs (Table 1), mixtures were made with *Opuntia ficus-indica* mucilage; *Aloe barbadensis* Miller mucilage as binder and emulsifier agents [27]; fructans were added as stabilizer, humectant, and gelling agents [28]; and fibrous material (FL and FC), that give different characteristics to the porous surface [29]. The mixture was kept under constant magnetic stirring while heating to 80 °C for 10 min. The suspension was emptied into Petri dishes and dried at 60 °C for 48 h in an oven (VWR Scientific Products) to obtain different LBMs, with an average thickness of 0.3422 mm.

Table 1. Composition of Lignocellulosic Biopolymer Membranes (LBMs).

Membranes	n	Composition			
		Fibrous Material (wt. %)	Mucilages (<i>Opuntia ficus-indica</i> and <i>Aloe Barbadensis Miller</i>) 1:1 (wt. %)	Fructans (wt. %)	Total Solids
FC30	3	30	39	31	100
FC50	3	50	32	18	100
FC70	3	70	25	5	100
FL30	3	30	39	31	100
FL50	3	50	32	18	100
FL70	3	70	25	5	100

2.3. Cytotoxicity Test by ISO: 10993-5: 2009

2.3.1. Cell Culture

For the cytotoxic evaluation, a cell line of normal primary dermal fibroblast was used: human, neonatal (HDFn) ATCC[®] PCS-201-010. The cell line was provided by the stem cell biology laboratory of the Faculty of Medicine of the Autonomous University of the State of Morelos, México. The cells were cultured, according to the ISO 10993-5:2009 protocol, in 2 mL of DMEM culture medium, which contains glucose, L-glutamine, sodium pyruvate, sodium bicarbonate, and sterile-filtered liquid, in 24-well plates at a density of 10,000 cells/cm². Human fibroblast cultures were propagated to obtain a semi-confluent density of 80% (4 days of culture). Subsequently, a sample of LBMs, previously bored to 6 mm Ø and sterilized with ultraviolet (UV) light for 30 min on each side, were isolated from moisture and covered with foil until used. They were deposited in Transwell-COL collagen-coated polytetrafluoroethylene (PTFE) inserts with 0.4 µm pore size and 6.5 mm diameter (Figure 1). The test was carried out in triplicate.

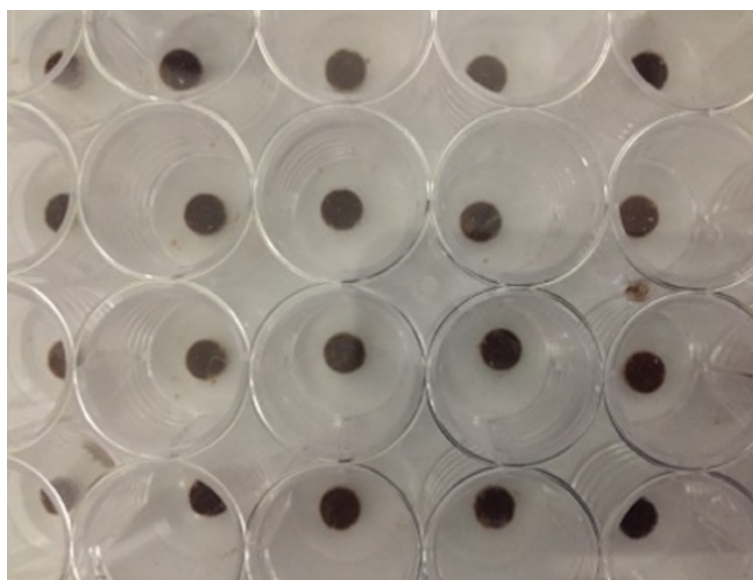


Figure 1. Lignocellulosic biopolymeric membranes 6 mm Ø deposited in transwell inserts in 24-well culture plate.

2.3.2. Cytotoxicity Test

The first evaluation was after 24 h of culture, allowing the adherence with the six different LBMs of 30 (FC30), 50 (FC50), and 70% (FC70) long fiber and 30 (FL30), 50 (FL50) and 70% (FL70) short fiber

in indirect contact using a transwell insert holder, so they did not have direct contact with the cells. Along with the addition of membranes and in order to have a positive control of oxidative stress, three culture wells with only cell culture medium were also subduced. The control group consisted of cells in culture medium, with normal growth to the same semi-confluent density and without exposition to the membranes. The cell densities used in each 24-well plate were the suggested: 10,000 cells/cm² cells). The test was carried out in triplicate. Membranes were removed one by one with dissecting forceps, and once this process was completed, cell cultures were fixed with 10% trichloroacetic acid for 1 h, followed by washing five times with distilled water at 4 °C, and dried at room temperature for 12 h.

2.3.3. Staining with Sulphordamine B (SRB)

Staining with SRB is a determination of the total protein content by staining with SRB (sulphordamine B), which is a bright pink aminoxantane dye with two SO³ sulfonic groups, which under moderately acidic conditions increase their affinity for the basic amino acids of proteins, electrostatically and selectively fixing them [30]. After 24 h of applying the treatment on the cells, the culture medium was extracted. Subsequently, 100 µL of 10% trichloric acetic acid (TCA) solution was added to each well and incubated for one hour at 4 °C. After the incubation time, the TCA was discarded and each plate was washed five times with 500 µL of distilled water at 4 °C, and at the end of the washings, it was allowed to dry for 12 h. Next, 300 µL of SRB solution was added to each well by incubating it for 30 min at room temperature.

Subsequently, the dye was removed by five washes per plate with 300 µL of 1% acetic acid. Finally, 100 µL of 10 mM base TRIS solution, pH 10, was added. Finally, the 24-well plates were placed for the quantification absorbance in a spectrophotometer (Synergy 2 BioTek). The absorbance plate test compares the reader's optical density to wavelength measurements from 200 to 999 nm in 1-nm increments.

To avoid the appearance of false positives in this assay because of the SRB dye binding to the amino acid residues of the proteins, transwell inserts were used within the 24-well plate, which allows the exchange of molecules between the different LBMs and the culture medium, since they have pores with a diameter of 0.4 µm, and also prevents the remains of the material being evaluated from adhering to the surface of the culture plates, thus preventing the formation of false positives due to their staining.

2.3.4. Viability

The viability of the cell culture exposed to the different LBMs, was compared against the control group. It was made using a Synergy 2 plate reader by recording absorbances. A reduction in the amount of protein in the sample results in a reduction in the number of living cells. This reduction is directly correlated with the amount of SRB formed by fluorescence. The viability [22] was determined and compared to the blank with the following equation:

$$\%Viability = (100 \times OD_{570e})/OD_{570b} \quad (1)$$

where:

OD_{570e} is the average OD of the respective groups that were in contact with different LBMs.

OD_{570b} is the average OD of all the wells of the control group. All values are final ODs after subtraction of background absorbance.

A tested LBM has cytotoxic potential when the cell culture viability decreases to <70% in comparison with the control group, which was set at 100% viability [22].

2.4. Assessment of Cytotoxicity According to ISO: 10993-5: 2009

2.4.1. Quantitative Evaluation

The average viability percentages were obtained for each concentration of fibrous material based on the outcomes of the three repetitions of each experiment [22]. The compared data were the cytotoxicity potentials obtained from different plate readings on the spectrophotometer and the fluorescence intensity by staining the cells. This established differences in response between the cell viability of each membrane, in the different samples evaluated, and determined if the methods provide comparable results in the viability of the exposed cells in the LBMs versus the viability of the cultures of cells of the control group.

2.4.2. Qualitative Evaluation

Culture wells were examined microscopically with fixed cells. Changes in general morphology, vacuolization, cell lysis, and LBM integrity were evaluated. The change in normal morphology was performed descriptively and numerically (Table 2), in accordance with the qualitative morphological classification of cytotoxicity in the standard [22].

Table 2. Degree of reactivity according to cell conditions.

Grade	Reactivity	Cell Conditions
0	None	Discrete intracytoplasmic granules, without cell lysis, without reduction of cell growth.
1	Slight	No more than 20% of the cells are round, freely bound and without intracytoplasmic granules, without changes in morphology; occasional lysed cells; a slight growth inhibition is observed.
2	Measured	No more than 50% of the cells are uniform, without intracytoplasmic granules, without extensive cell lysis; no more than 50% inhibition of observable growth.
3	Moderate	No more than 70% of the cell layers contain rounded cells or these are lysed; cell layers are not completely destroyed, but more than 50% growth inhibition is observed.
4	Severe	Almost complete or complete destruction of cell layers.

2.4.3. Environmental Scanning Electron Microscopy

The surface of the obtained short and long LBMs was observed by means of environmental scanning electron microscopy (Zeiss, Evo LS10, Munich, Germany), to determine the distribution and conformation of the dressing.

2.4.4. Fourier Transform Infrared Spectroscopy

The functional groups of the short and long mixtures of the obtained LBMs were determined using ATR-FTIR. A Shimadzu spectrophotometer (IR Affinity model, Shimadzu, Japan), equipped with ATR (attenuated total reflection), was used with the following scanning parameters: zinc selenium crystal, % transmittance, number of scans: 100, 4 cm⁻¹ resolution. The region that was used for the analysis was 500–4000 cm⁻¹. The dried and sterilized membranes were mounted on the equipment sample plate. From the transmittance spectra, it was possible to identify interactions between the used biopolymers.

2.4.5. Adsorption of Ultraviolet Radiation

The UV radiation adsorption of the different LBMs was determined using an EA30-Extech Lux meter (8-volt UVL-28 UV lamp). The amount of light transmitted on the different exposed membranes

was quantified for about 2 s. The LBMs were exposed to different wavelengths, 254, 302, and 365 nm, covering the entire spectrum of UV light radiation, and the tests were performed in triplicate for each concentration. The lux meter detector was completely covered and the lamp was placed 24 cm away from the detector, inside a black box to eliminate external light.

2.4.6. Image Texture Analysis

Stereoscopic surface microscopy can be analyzed as a set of rectangular images N_z (layers) with N_x pixels in the horizontal direction and N_y pixels in the vertical direction. The digital value of each pixel is quantified to N_g gray levels: $L_x = \{0, 1, \dots, N_x - 1\}$, $L_y = \{0, 1, \dots, N_y - 1\}$, and $L_z = \{0, 1, \dots, N_z - 1\}$ with domains X , Y , and Z . In addition, $G \in \{0, 1, \dots, N_g - 1\}$ is the set of N_g gray levels. The set $L_x \times L_y \times L_z$ is the set of pixels of the images ordered by their column-row-layer designations. The images can be represented as a function that assigns some digital value in G to each pixel in $L_x \times L_y \times L_z$; $I: L_x \times L_y \times L_z \rightarrow G$ [31]. Therefore, an image can be represented as a function, which assigns various shades of gray for each pixel or set of pixels, and from this information you can characterize the texture of an image [32].

In a two-dimensional gray level histogram for a pair of pixels (reference pixel and neighbor), this matrix approximates the probability of joint distribution of a pair of pixels [33].

The texture is quantified by a set of continuous variables, which describes the local spatial arrangement of reflectance values. Texture measurements describe quantitatively the relationships among the N_z values of the neighboring pixels. The result is a continuous measurement of spatial information that can be used for further processing. Spatial relationships are not necessarily correlated with the spectral data for a given class, and the inclusion of a measure for them improves the accuracy of the classification [34].

The second angular momentum (SMA) or energy parameter measures the textural homogeneity of the image and is a parameter opposite to entropy. The contrast, which is also known as variance or inertia, is a measure of the local variations of the grayscale values of the image pixels. Entropy, which measures the disorder or randomness of the images and characterizes the texture of the image, is an indication of the complexity within the image. Therefore, complex images will have high entropy values [35].

Finally, the fractal dimension performs a description of irregular objects. This refers to the description of irregular geometry or fragmented forms of natural characteristics, as well as other complex objects that traditional Euclidean geometry cannot analyze [36]. It is an ideal tool to measure the roughness/texture of an image [37].

Image texture analysis (ATI) was used to characterize quantitatively the surface microstructure of different LBMs. Five study parameters were obtained: fractal dimension (DFT), energy (or second angular moment), contrast and entropy. All images obtained from microscopy (ESEM) were converted to grayscale images. Subsequently, algorithms of the gray level co-occurrence matrix (GLCM) and shifting differential box counting (SDBC) were applied to obtain texture parameters from grayscale images [38]. All image processing was performed using the Image J v1.34 software program. Five texture parameters were extracted from images obtained from microscopy techniques with the GLCM texture plug-in included in the Image J software program, as well as the SDBC plug-in for calculating the fractal dimension (DFT).

The values of the different parameters obtained were averaged with their respective standard deviations (average \pm standard deviation), obtained from equations [30] for the texture parameters extracted from grayscale SEM images. Statistical values were obtained using one-way analysis of variance (ANOVA) followed by the multiple comparison test with Minitab v.15 statistical software. Significant differences were considered when $p \leq 0.05$. The graphs and equations of the results were generated using SigmaPlot v.11 software (Systat Software Inc., San Jose, CA, USA).

3. Results

3.1. Assessment of Cytotoxicity According to ISO: 10993-5: 2009

3.1.1. Quantitative Evaluation

The data presented represent the average of three repetitions of LBMs cytotoxicity assays using the SRB method, and the error bars indicate the standard deviation (Figure 2). The standard deviation remains with little dispersion in all samples and the cytotoxic effect is found in acceptable limits. If the viability is reduced to <70% of the control; it had a cytotoxic potential [22], with the exception of the SF30 membrane, with a cytotoxicity of 64.64%. All other samples showed values higher than 70% (Table 3).

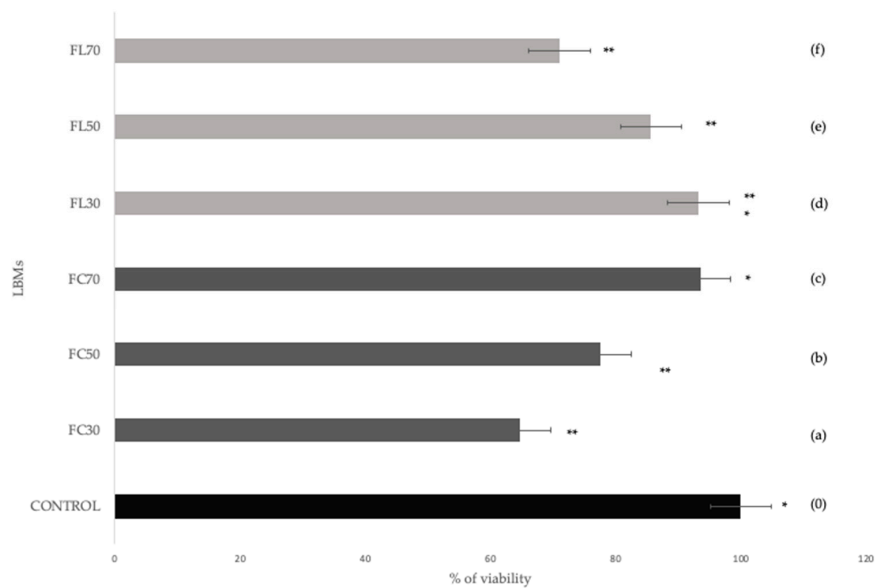


Figure 2. Average cytotoxic evaluation of LBMs in human fibroblast culture medium during the three cytotoxicity evaluations. Associated with the micrographs of Figure 3, (*, **) values with different sets are significantly different at p -value < 0.05 in the bilateral equality test for column means. The tests assumed equal variances.

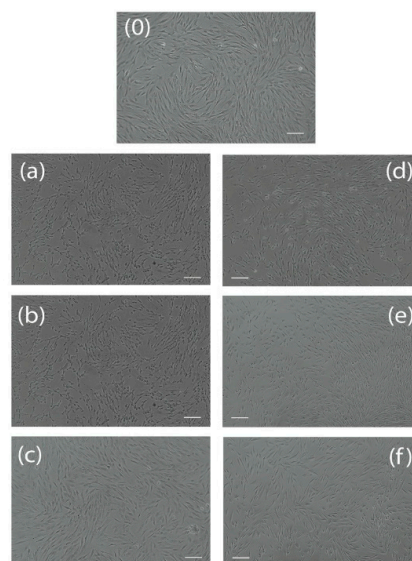


Figure 3. Stereotypical micrographs of the different fibroblast culture media evaluations of all LBMs: 0 control group, (a) FC30, (b) FC50, (c) FC70, (d) FL30, (e) FL50, and (f) FL70. Bar 100 µm.

Table 3. Average cytotoxic evaluations of the mixtures using the Sulphordamine B (SRB) method.

Membranes	Viability Media	Cytotoxicity
CONTROL	100.00 ^a	Viable
FC30	62.12 ^b	Not viable
FC50	71.59 ^b	Viable
FC70	80.84 ^a	Viable
FL30	79.51 ^{a,b}	Viable
FL50	75.56 ^b	Viable
FL70	61.13 ^b	Not viable

(^{a,b}) values with different letters are significantly different at p -value < 0.05 in the bilateral equality test for column means. Tests assumed equal variances.

The different membranes showed a concentration-response relationship since cytotoxicity increased gradually with increasing concentration of the fibrous material. The result of the one-way ANOVA test shows (Table 3) that there is no significant difference between the cell viability and the different treatment conformations at probability value ($p > 0.05$).

Cytotoxicity evaluations performed in LBMs, for both LF and SF, at different concentrations were shown to have mild cytotoxic activity [22]. Using an average of the three evaluations of all the LBMs, an acceptable behavior of obtained results according to ISO: 10993-5:2009 is observed. A cytotoxic viability behavior of 64.64 and 77.65%, respectively, is observed in the sieved dressings FC30 and FL50. However, the SF70 sample reaches 93.52% cell viability—the lower the agavaceous load, the lower cell viability. On the other hand, the LBMs without screening have a downward behavior with FL30, FL50, and FL70, showing a cell viability of 93.18, 85.66, and 71.09%, respectively. The lower the agavaceous load, the greater the cell viability, which could indicate that the screening process could reduce the concentration of some types of toxic contaminant (Figure 2).

Larger particles have a smaller surface area and lower porosity among the particles, in contrast to small particles that have a larger specific surface area with less porosity within it [39]. Since LBMs have a greater specific area with screened fibers, because of the particle size, they are provided with a better distribution, which leads to better cell growth.

3.1.2. Qualitative Evaluation

The morphology change is shown descriptively and numerically (Table 4), according to the qualitative morphological classification of cytotoxicity of extracts (Table 2) [22]. Figure 3 shows the micrographs with an inverted microscope (Nikon eclipse ts100, Tokyo, Japan) at 10× magnification of the different fibroblast culture media evaluations of all the LBMs.

Table 4. Morphological conditions of cell cultures.

Grade	Reactivity	Cell Conditions
1	Slight	No more than 20% of the cells are round, freely bound and without intracytoplasmic granules, without changes in morphology; occasional lysed cells; a slight growth inhibition is observed.

3.2. Environmental Scanning Electron Microscopy

In Figure 4, the surfaces of the different screened and unscreened LBMs are shown at 30,50,70% fibrous material, respectively. It is evident that membranes show completely different surface morphologies. ESEM micrographs of the longitudinal sections of the LBMs show the conformation between natural binders and lignocellulosic materials (fiber matrix), forming porous structures.

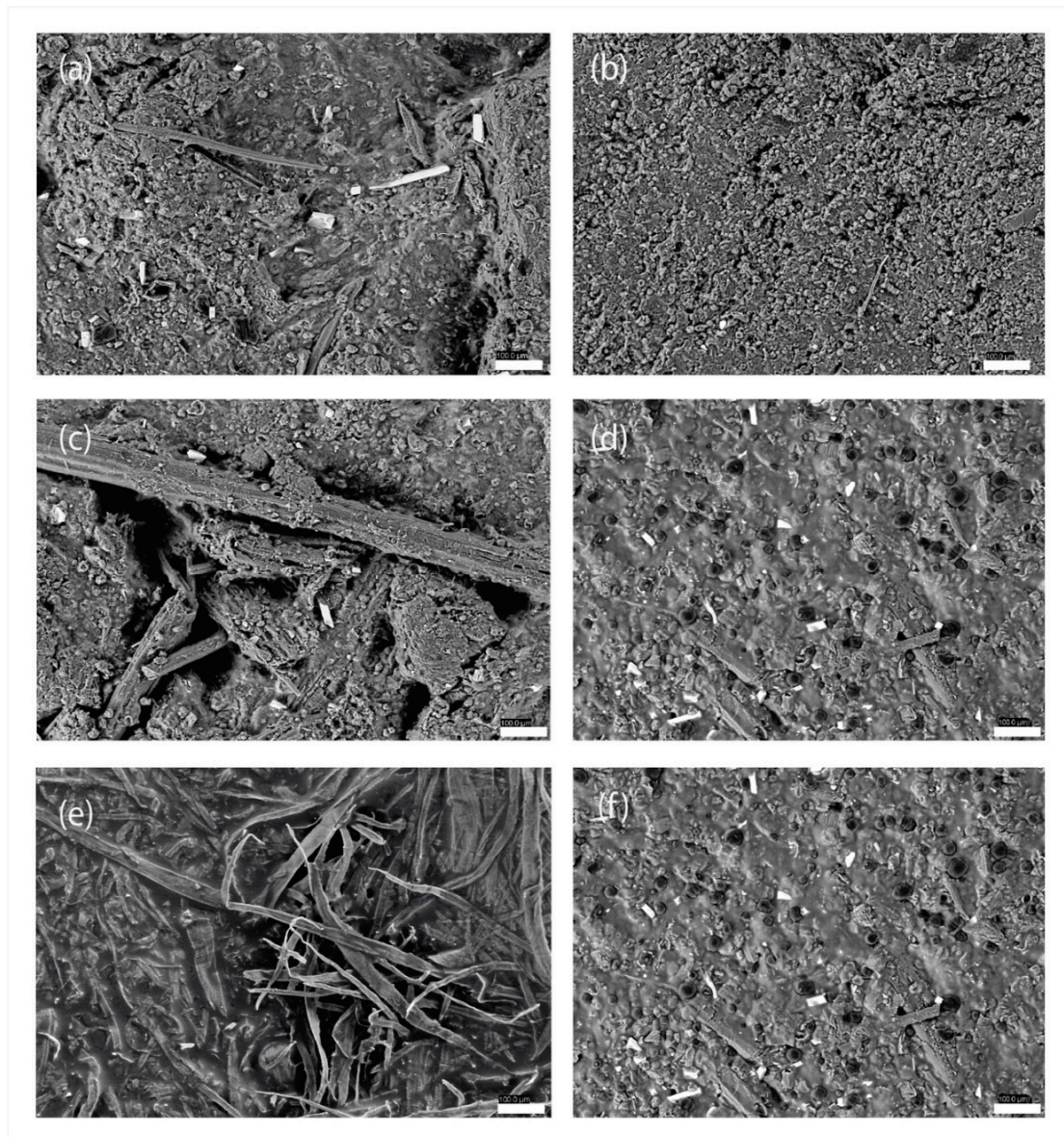


Figure 4. Scanning Electron Microscope (SEM) images of LBMs (a) FL30, (b) FC30, (c) FL50, (d) FC50, (e) FL70, and (f) FC70. The bar corresponds to 100 μm , 60 \times magnification.

3.3. Fourier Transform Infrared Spectroscopy

Figure 5 shows the FTIR spectra of different LBMs where the detection of phenol-OH corroborates the presence of the conjugation in the molecular structure of the components of the LBMs, attributing to them the absorption potential of UV radiation.

An analysis of the spectra was performed and identified chemical groups in different frequency ranges are shown in Table 5.

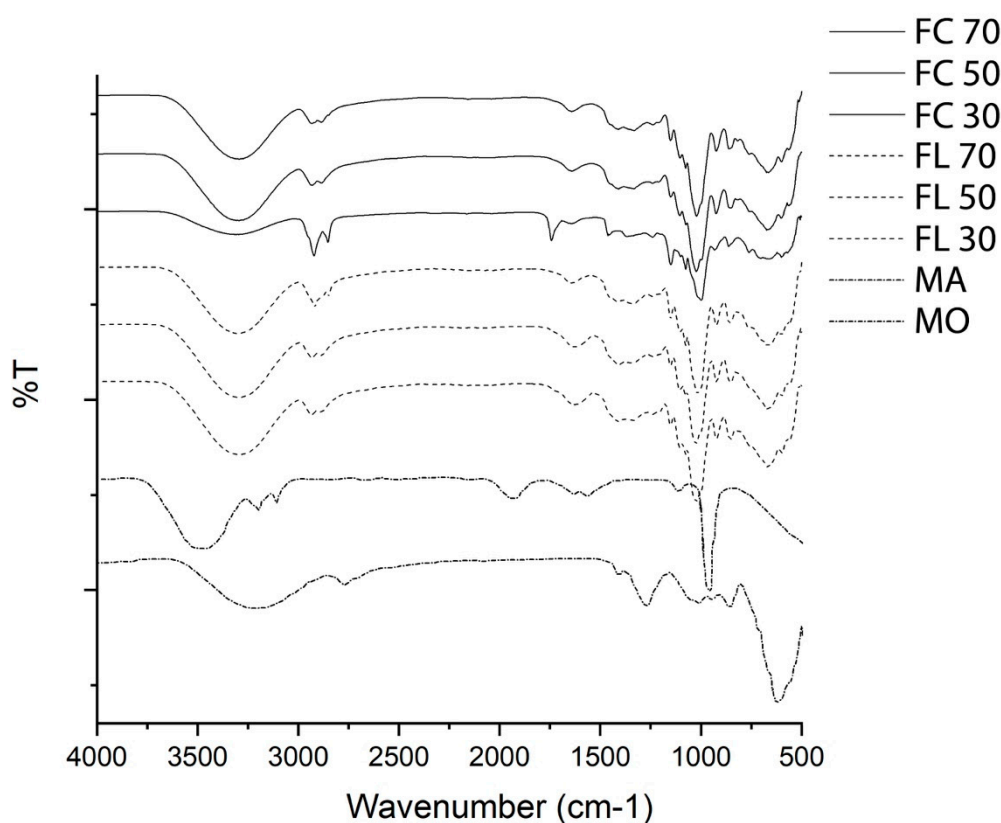


Figure 5. FTIR spectra of different LBMs obtained (MA: *Aloe barbadensis* Miller mucilage; MO: *Opuntia ficus-indica* mucilage).

Table 5. Infrared absorption bands for the different LBMs.

Wave Number (cm ⁻¹)	Vibration Mode	Functional Groups
3600 and 3200 cm ⁻¹	Stretching of the phenolic OH group	Specific phenols of aloe, including flavonoids, flavonols.
2900–2936 cm ⁻¹	C-H bond stretching of carbohydrates. Flexion belonging to C-O-H, C-O-C bonds	Oligosaccharides and polysaccharides.
1608 cm ⁻¹	Plane bending C = C bonds of lignin molecules.	Depending on the concentration and if it was LMB FC and FL.
1870–1540 cm ⁻¹	Ketones carbonyl group	Ketones with possible keto enolic balances.
650–1580 cm ⁻¹	Stretch = CO	Amino acids and polysaccharides.
700–650 cm ⁻¹	Acetyl groups	These grant biological activity
1185–1045 cm ⁻¹	Stretch (CO, ether bond) and the pyranoid rings (CC) stretch	Stretching of glycosidic bonds (CO, ether bond) and pyranoid rings (CC) attributed to polysaccharides that are part of pectins and mucilage.
3298 cm ⁻¹	Stretching of the hydroxyl groups, -OH	Carboxylic acids, amino acids, alcohols, and water molecules.

3.4. Adsorption of Ultraviolet Radiation

UV absorption profiles at different wavelengths. The percentage of UV light absorbance in FL membranes was between 51.56% and 82.45%. The FL70 membrane had the highest value. The absorbance activities of the LBM FC had absorbances between 29.43% and 52.01%. The lowest value was shown by the FC 30% mixture.

LBM with long fibrous material exhibited better UV light absorbance, indicating better material distribution compared to LBM with FC material. It is observed that membranes with a higher content of fibrous material can prevent the passage of UV light towards the lux meter, which increases the absorbance intensity.

The different membranes showed a concentration-response relationship since the UV absorbance increased gradually with increasing concentration of the fibrous material. The result of the one-way ANOVA test shows that there is no significant difference among different wavelengths, but in the conformation, they are significantly different at p -value ($p > 0.05$), as is shown in Table 6.

Table 6. UV absorbance after exposure to different wavelengths of different LBMs with the different concentrations (30, 50 and 70%).

		Wavelength									
		365 nm UV Long			302 nm UV Middle			254 nm UV Short			
		% Fiber			% Fiber			% Fiber			
		30	50	70	30	50	70	30	50	70	
		Media	Media	Media	Media	Media	Media	Media	Media	Media	
UV Absorbance	Conformation	FC *	47.89 ^a	34.89 ^b	29.43 ^c	50.21 ^a	45.12 ^b	37.23 ^c	51.79 ^a	52.01 ^a	45.35 ^b
		FL **	70.56 ^a	62.90 ^b	51.56 ^c	75.21 ^a	70.24 ^b	59.12 ^c	82.45 ^a	81.98 ^a	74.99 ^b

(^{a,b,c}) values in the same row and subtable, which do not share the same subscript, are significantly different at p -value < 0.05 in the bilateral equality test for column means. Boxes without a subscript are not included in the test. Tests assume equal variances. (*,**) The values of different row and subtable, which do not share the same subscript, are significantly different in the p value < 0.05 in the bilateral equality test for the means between the rows.

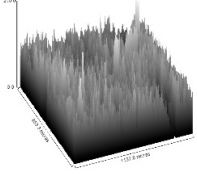
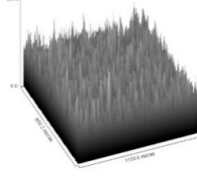
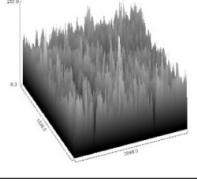
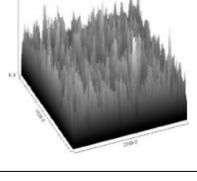
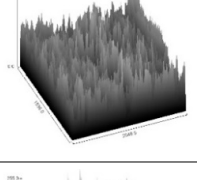
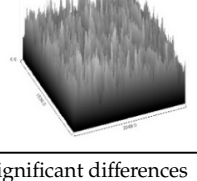
3.5. Image Texture Analysis

The texture of the images was analyzed by studying the spatial dependence of the pixel values represented by a coincidence matrix P_d, θ with entry in $P_d, \theta (i, j)$ is the frequency or relative distance for two pixels (d) in the direction θ that has i and j values, respectively. These parameters were calculated at a pixel pitch “ d ” equal to 1 and with a displacement angle “ θ ” of 0° [40]. Table 7 shows the results of the study parameters fractal dimension (DFT), energy (or second angular moment), contrast and entropy.

The co-occurrence matrix is a frequency matrix with which a pixel with a gray level (i) appears in a specific space relationship with another gray level pixel (j). The concurrence matrices are second order measures because they consider pairs of neighboring pixels, separated by a distance d and at a certain angle. Therefore, the occurrence matrices can reveal certain properties in the spatial distribution of the grays in the texture of the image [41].

A fractal entropy/dimension ratio was also calculated. This correlation between entropy and the fractal dimension is inverse: the higher the value of the fractal dimension, the lower the value of the entropy, that is to say, the more homogeneous the image is. This relationship was estimated as the ratio of the entropy values divided into the fractal dimension values calculated from the same image [42]. Therefore, higher values of the entropy/fractal dimension relationship will be related to images with a high degree of complexity and roughness, while low values may be associated with simple and smooth images. Thus, an adequate correlation is shown among the fiber load content parameters of the different LBMs.

Table 7. Analysis of texture images of the ESEM micrographs of the LBMs (SMA: second angular momentum).

	DFT	Contrast	Entropy	SMA	Entropy/DFT Relation	
FL30	2.56215 ^{a,b,c}	187.93 ^{a,b}	8.9805 ^{a,b}	0.000245 ^{a,b}	3.50506	
FC30	2.6462 ^a	311.902 ^a	9.393 ^a	0.000569 ^{a,b}	3.54961	
FL50	2.5922 ^b	214.2285 ^{a,b}	9.042 ^b	0.000381 ^{a,b}	3.48815	
FC50	2.5896 ^{a,b,c}	215.95 ^{a,b}	9.1265 ^{a,b}	0.00025 ^{a,b}	3.52428	
FL70	2.5313 ^c	183.5485 ^b	8.996 ^{b,c}	0.000182 ^a	3.55390	
FC70	2.5948 ^{a,b,c}	222.6915 ^{a,b}	9.157 ^{a,b}	0.000238 ^b	3.52898	

^(a,b,c) values (average \pm standard deviation, $n = 5$) in a column with the different letters show significant differences ($p < 0.05$).

4. Discussion

4.1. Assessment of Cytotoxicity According to ISO: 10993-5: 2009

Quantitative and Qualitative Evaluation

Cytotoxicity assays performed on the FC and FL membranes at different concentrations showed that almost all evaluated LBMs have an acceptable viability. Only two membranes were below the viability threshold, FL70 (61.13%) and FC30 (62.12%), according to ISO: 10993-5: 2009. The FC30 mixture showed the lowest viability percentage of the LBMs evaluated, reaching 62.12%, while the FC70 sample showed the highest percentage of viability (80.84%). However, due to sample size and

media volume as well as direct contact and lack of evidence of adherence, this would be a preliminary *in vitro* evaluation.

In stereotypically observed micrographs (Figure 2) of the different cytotoxicity evaluations, the fibroblast culture media are observed in a typical arrangement, in the form of a spindle with a distance growth similar to that of the control or blank in the cases of FC samples. The zone of inhibition and minimization of growth was less obvious in the case of FC30 and FC50.

For the FL50 and FL70 membranes, a large number of many devitalized cells are observed in the vicinity of the material, as well as small areas of inhibition. In this case, the cell is adopting a contracted form, which would indicate a low adhesion with the scaffolding material. Clear differences are observed among the morphologies adopted by the cells in these samples, leading to the conclusion that cell adhesion depends on the physicochemical characteristics of the surface of the material [43]. Lignocellulosic fibers have hygroscopic properties [44]. This is consistent with many results in which different cell lines showed variable adhesion based on surface wettability [45]. Cells have been considered to generally adhere better to moderately hydrophilic surfaces compared to hydrophobic or hydrophilic ends [46].

The qualitative cytotoxic behavior was classified as mild reactivity since no more than 20% of the cells are round, freely bound and without intracytoplasmic granules, and these do not show changes in morphology (Table 3); a slight inhibition of the growth of occasional lysed cells is observed. LBMs showed considerable swelling due to the absorbed culture medium because of the insert. In the case of the FC30 membrane, there was a deformation and shedding of it. Some results have showed that LBMs do not produce cytotoxic effects in indirect contact with the culture of fibroblast cells *in vitro*, since no major malformation, degeneration, propagation, or lysis of fibroblast cells was observed according to stereoscopic micrographs [47].

Any cytotoxic effect may be cause for concern. However, it is primarily an indication of the potential for *in vivo* toxicity, and it cannot be determined necessarily that the device is unsuitable for a given clinical application, based solely on cytotoxicity data [22]. Consequently, the results of *in vitro* cytotoxicity tests should be viewed in a complementary context of biocompatibility tests performed on these membranes to obtain a more accurate assessment of the biological risk associated with Eastern clinical use [21].

4.2. Environmental Scanning Electron Microscopy

The use of ESEM in this study allowed the visualization of LMB FL, which have a very rough and porous structure; they are more irregular and full of fibers, showing wide cavities delimited by fibers. A crossing of the structure with crosses and valleys is observed. The pores were larger with more irregularity in shape. On the other hand, LBM FC show a smoother structure with a more uniform texture, a more regular surface without fibers, and no apparent cavities in the amplification used. In other studies, similar observations were made [48] with Agave and polyethylene fiber composites produced by compression molding.

ESEM micrographs of the longitudinal sections of the LBMs show the conformation between natural binders and lignocellulosic materials (fiber matrix), forming porous structures. These interactions between fibrous material and mucilages is certainly due to the formation of an interwoven network between both biopolymers with similar structural and chemical characteristics [49].

Both conformations show porosity. The LBM FL exhibited a more porous network within the composite matrix. The property of porosity (Figure 3) in a biomaterial extends the scope of applications. In porous biopolymers, you can find closed (isolated) pores and open (connected) pores. Pore interconnectivity is important for the accessibility of gas, liquid, and particle suspensions [50], and even for the incorporation of cell populations [51]. The pore structure in LBM LF has greater penetrability of substances and possible interactions between compounds, giving it impact characteristics in tissue engineering applications, since the behavior of cell/tissue growth depends on a porous structure [50].

The membranes of short fibers and long fibers are porous materials with micro and nano pores made of natural polymers that are of special interest for medical, cosmetic, pharmaceutical, and other applications where biocompatibility and biodegradability are required [52].

4.3. Fourier Transform Infrared Spectroscopy (FTIR)

The absorption peaks between 700 and 650 cm^{-1} are due to the presence of acetyl groups that grant biological activity. Due to the abundance of hydroxyl groups, when there is cross-linking, a conformational variation of the polymer begins and the polymer may act in such a way that hydroxyl groups are exposed [53], thus showing cross-linking of the membranes. These spectra indicate that obtained LBMs contain a variety of functional groups such as carbonyls, amino acids, hydroxyls, aldehydes, anthraquinones, and effective cross-linking agents [54], which suggests their possible use as an alternative for human topical use.

The absorption band between 1185 and 1045 cm^{-1} is related to the stretching vibrations of the glycosidic bonds (CO, ether bond) and the pyranoid rings (CC) attributed to the polysaccharides that are part of the pectins of the mucilage [55,56].

Stretch groups = CO were observed from 650 to 1580 cm^{-1} , indicating the presence of carbonyl compounds, amino acids, and polysaccharides, which coincides with what was reported in [57]. The spectral characteristic bands of the C = C ring are observed at 1608 cm^{-1} [58].

The stretching of the phenolic OH group in the absorption bands around 3600 and 3200 cm^{-1} explains the presence of aloe-specific phenols, including flavonoids, flavonols, phenolic anthraquinones, etc. These have application as corrosion inhibitors [59].

Biochemicals are important in the composition of the medicinal attributes of aloe (in addition to enzymes, minerals, amino acids, and some vitamins) [60]. The peaks of the 2900–2970 cm^{-1} region belong to the stretches that have the stretching links of the CH bond of carbohydrates and a flexion that belongs to the COH, COC bonds, which are characteristic of various oligosaccharides and polysaccharides. The spectrum showed a change in intensity at the peak around 1593, depending on the concentration and whether it was LBM FC or LBM FL, as part of the C = C bonds of the lignin molecules [61].

The band around 3276 cm^{-1} is mainly related to the vibration of the intramolecular hydrogen bond stretch of the amino group of amide A, while the observed band around 2936 cm^{-1} is assigned to the C-H stretch of the amide B [62].

The band around 3298 cm^{-1} is mainly related to the stretch bands of the hydroxyl groups, -OH, of carboxylic acids, amino acids, alcohols, and water molecules [58].

4.4. Adsorption of Ultraviolet Radiation

From the tested LBMs (Table 6), a UV light absorption potential from 29.43 to 52.01% was observed in FC membranes and a greater potential for UV light absorbance was observed in FL membranes (from 51.56 to 82.45%). This could be due to lower solubility and higher concentration and dispersion of components over the entire surface. This behavior is because secondary metabolites such as flavonoids and esters in plant leaves can absorb UV radiation [63,64]. Presumably, the polyphenols in the Aloe extracts were the main UV absorbing elements. Aloe gel is believed to have a modulating effect on the skin by preventing sunlight from sensitizing the skin, especially in the first 24 h after exposure [65]. This is corroborated in the FT-IR results, by showing bands associated with Aloe.

Since UV radiation penetrates deeply, affecting the dermis, destroying elastic and collagen fibers, and conditioning aging, immune suppression, photoallergic reactions, and phototoxic reactions [66], a full scan of the UV radiation spectrum was performed. However, the behavior of the percentage of UV light absorbance in both the LBM FC and FL do not show significant differences in the evaluation of the near, medium, and far UV spectrum.

Due to its phenolic structure, both lignin and Aloe vera provide the membrane with light-absorbing properties, a natural potential for protection against UV rays, while also presenting stability against

thermal oxidation when present in mixtures with other polymers. Previous research has modified the potential of lignocellulosic materials as a component in UV light-blocking membranes [67].

In addition to this, considering the impediment of the passage of UV radiation through the treated fibrous material, this gives the property of sunscreens, which absorb and/or prevent UV radiation from reaching the skin. The link between chronic human skin exposure to the sun and harmful clinical consequences such as photoaging and skin cancers is indisputable. Sun exposure can quickly induce well-characterized and visible clinical consequences, such as sunburn [68].

4.5. Analysis of Image Texture

The texture parameters adequately described the texture of the membranes observed with ESEM microscopy (Table 7).

Regarding contrast, LBM FL had the highest values compared to LBM FC. High contrast values measured in the LBM FC are associated with the fibrillar microstructure formed in the membranes. This is attributed to a greater presence of fibers, which causes the contrast values to increase, which indicates a high degree of local variation of pixels within the image [17].

The highest value of the entropy parameter (9.35) corresponded to LBM FC30, which indicates an inhomogeneous surface. The lowest entropy values were obtained with LBM FL30, which means that its surface texture is more homogeneous.

Finally, the fractal dimension values for all LBMs can be associated with the roughness observed in their respective images, where LBM FC30 (more homogeneous surfaces) had the highest fractal dimension value (2.6452), while low values were observed. (2.5261) for LBM FL70 (heterogeneous surfaces). A roughened surface becomes more susceptible to decay and may fragment. Ultraviolet radiation from sunlight initiates a wide variety of chemical changes in surfaces, which causes them to deteriorate, thus losing their usual appearance and also their mechanical properties, as the strength characteristics are degraded [69]. High roughness could reduce UV light transmission through higher light reflection.

The entropy/fractal dimension relationship values for LBM FC30 (3.5496) and FL70 (3.5539) are related to images with a high degree of complexity and roughness, while LBMFC 50 (3.5242) and FC70 (3.5289) have lower values, which are associated with simpler and smoother images. This fact is associated with the structural complexity observed in the topographic images of the LBM surfaces. This was mentioned in previous works, in which the effect of the addition of surfactants and optical parameters on the microstructure of hydroxypropyl methylcellulose films was studied [70]. Using microscopic characterizations, the complexity of the film surfaces was evaluated using the fractal dimension parameter.

Therefore, it can be said that the texture analysis of images is a complementary tool for qualitative studies of the morphologies of the surface of biomaterials, in addition to having the advantages of being an economic and fast tool, which allows the analysis of samples with larger surfaces [30].

5. Conclusions

FC70 and FL30 membranes were not a significant difference between cell growing control. They had 10,000 cells/cm² in the culture of normally growing primary dermal fibroblast. In this study, particle size was relevant in the FC membranes because better distribution and a greater contact area provided a greater interaction with the culture medium, which leads to better cell viability (93.52%) in respect to FL membranes. These results for FC70 and FL30 membranes correlated with the image analysis of texture from the ESEM micrographs and FT-IR spectrophotometry.

The particle size in the FL membranes established a high level of porosity, lower solubility, and a higher solid concentration and dispersion. These aspects were related to greater potential for UV light absorption in FL membranes for all the different wavelengths, 254, 302, and 365 nm, covering the entire spectrum of UV light radiation. However, FL70 membrane had the greatest potential for UV light absorption with 82.45% absorbance at 254 nm of UV light radiation.

The main advantage of this proposal was the incorporation of native vegetation in LBM membranes with Agave fiber and mucilages as natural binders. The conformation of these membranes shows a promising alternative as dermal dressing.

Author Contributions: Conceptualization: L.A.G.S., B.H.C.D. and M.A.G.d.A.M.; investigation, J.M.M. and M.Á.R.L.; writing—review and editing, L.A.G.S., B.H.C.D. and M.A.G.d.A.M.; funding, L.A.G.S., B.H.C.D., A.R.J.A. and J.S.-O.T. All authors have read and agreed to the published version of the manuscript.

Funding: This research received no external funding.

Acknowledgments: The first author is grateful for the support of the National Council of Science and Technology (CONACYT) for the scholarship granted to pursue a PhD in sciences in conservation of landscape heritage within the doctoral program of the CeProBi and CIEMAD of the National Polytechnic Institute included in the registry of Postgraduate of Excellence and to the Autonomous University of the State of Morelos, especially to the Faculty of Medicine, to the laboratory of permaculture and eco design of nano microfibers at the Interdisciplinary Center for Research and Studies on Environment and Development-IPN, and to the CNMN-IPN National Multidisciplinary Laboratory of Materials Characterization. The authors acknowledge the support of the research at IPN under the projects SIP-20160103 and SIP-20181976.

Conflicts of Interest: The authors declare no conflicts of interest.

References

1. Oviedo Prieto, R.; Herrera Oliver, P.; Caluff, M.G. National list of invasive and potentially invasive plants in the Republic of Cuba 2011. *Bissea Boletín Sobre Conservación Plantas Jardín Botánico Nacional Cuba* **2012**, *6*, 22–96.
2. De Rzedowski, G.C.; Rzedowski y colaboradores, J. *Flora fanerogámica del Valle de México*, 2nd ed.; y Comisión Nacional para el Conocimiento y Uso de la Biodiversidad: Pátzcuaro, Michoacán, México, 2005; p. 1406.
3. Olivera, A.; Caballero Caballero, M.; Alavez Ramírez, R. Biocomposite tepexil cement reinforced with fibers of Agave angustifolia Haw as a light mortar. *Rev. Mex. Cienc Agric.* **2018**, *21*, 4406–4415. [[CrossRef](#)]
4. Agrawal, C.; Ong, J.; Appleford, M.; Mani, G. *Introduction to Biomaterials: Basic Theory with Engineering Applications*; Cambridge University Press: Cambridge, UK, 2019; pp. 19–47.
5. Pignatello, R. *PLGA-Alendronate Conjugate as a New Biomaterial to Produce Osteotropic Drug Nanocarriers*; Biomaterials Applications for Nanomedicine; InTech: Milan, Italy, 2011; pp. 165–184. [[CrossRef](#)]
6. Sunita, V.; Shivaram, S.; Sharma, C. Recent Advances in Biomaterials Science and Engineering Research in India: A Minireview. *ACS Biomater. Sci. Eng.* **2019**, *5*, 3–18. [[CrossRef](#)]
7. Parida, P.; Behera, A.; Chandra Mishra, S. Classification of Biomaterials used in Medicine. *Int. J. Adv. Eng. Sci. Appl. Math.* **2012**, *1*, 125–129. [[CrossRef](#)]
8. Vert, M. Biopolymers and Artificial Biopolymers in Biomedical Applications, an Overview. In *Biorelated Polymers*; Chiellini, E., Gil, H., Brauneegg, G., Buchert, J., Gatenholm, P., Van Der Zeem, M., Eds.; Springer: Boston, MA, USA, 2001; pp. 63–79.
9. Velasco, M.; Narvaez-Tovar, C.; Garzon-Alvarado, D. Design, Materials, and Mechanobiology of Biodegradable Scaffolds for Bone Tissue Engineering. *Biomed. Res. Int.* **2015**, *2015*, 1–21. [[CrossRef](#)]
10. Momoh, F.U.; Boateng, J.S.; Richardson, S.C.W.; Chowdhry, B.Z.; Mitchell, J.C. Development and functional characterization of alginate dressing as potential protein delivery system for wound healing. *Int. J. Biol. Macromol.* **2015**, *81*, 137–150. [[CrossRef](#)]
11. Pina, S.; Ribeiro, V.; Marques, C.F.; Maia, F.R.; Silva, T.H.; Reis, R.L.; Oliveira, J.M. Scaffolding Strategies for Tissue Engineering and Regenerative Medicine Applications. *Materials* **2019**, *12*, 1824. [[CrossRef](#)]
12. Sikareepaisan, P.; Ruktanonchai, U.; Supaphol, P. Preparation and characterization of asiaticoside-loaded alginate films and their potential for use as effectual wound dressings. *Carbohydr. Polym.* **2011**, *83*, 1457–1469. [[CrossRef](#)]
13. Vainio, H.; Bianchini, F. Cancer-preventive effects of sunscreens are uncertain. *Scand. J. Work Environ. Health* **2000**, *26*, 529–531. [[CrossRef](#)]
14. Ebrahimzad, M.A.; Enayatifard, R.; Khalili, M.; Ghaffarloo, M.; Saeedi, M.; Charati, J.Y. Correlation between Sun Protection Factor and Antioxidant Activity, Phenol and Flavonoid Contents of some Medicinal Plants. *Iran. J. Pharm. Res.* **2014**, *13*, 1041–1047. [[CrossRef](#)]

15. Gonzalez-Pumariiega, M.; Vernhes Tamayo, M.; Sanchez-Lamar, A. Ultraviolet radiation and its incidence in the human health. *Theoria* **2009**, *18*, 69–80.
16. Sordo, C.; Gutierrez, C. Skin cancer and sun radiation: Peruvian experience in the prevention and early detection of skin cancer and melanoma. *Rev. Peru. Med. Exp. Salud Publica* **2013**, *30*, 113–117. [[CrossRef](#)] [[PubMed](#)]
17. Wang, F.; Yao, J.; Chen, H.; Chen, K.; Trebše, P.; Zaray, G. Comparative toxicity of chlorpyrifos and its oxon derivatives to soil microbial activity by combined methods. *Chemosphere* **2010**, *78*, 319–326. [[CrossRef](#)] [[PubMed](#)]
18. Wang, M.O.; Etheridge, J.M.; Thompson, J.A.; Vorwald, C.E.; Dean, D.; Fisher, J.P. Evaluation of the In Vitro Cytotoxicity of Cross-Linked Biomaterials. *Biomacromolecules* **2013**, *14*, 1321–1329. [[CrossRef](#)]
19. Lozaga, G. *Cultivo de Células Animales y Humanas: Aplicaciones En Medicina Regenerativa*; Editorial Visión Libros: Madrid, Spain, 2011; Available online: <https://books.google.com.mx/books?id=Z3t4R39FByYC> (accessed on 28 February 2019).
20. Willershausen, B.; Marroquin, B.B.; Schafer, D.; Schulze, R. Cytotoxicity of Root Canal Filling Materials to Three Different Human Cell Lines. *J. Endod.* **2000**, *26*, 703–707. [[CrossRef](#)]
21. Liu, X.; Rodeheaver, D.P.; White, J.C.; Wright, A.M.; Walker, L.M.; Zhang, F.; Shannon, S. A comparison of *in vitro* cytotoxicity assays in medical device regulatory studies. *Regul. Toxicol. Pharmacol.* **2018**, *27*, 24–32. [[CrossRef](#)] [[PubMed](#)]
22. International Standard ISO 10993-5. *Biological Evaluation of Medical Devices—Part 5: Tests for In Vitro Cytotoxicity*, 3rd ed.; ISO: Geneva, Switzerland, 2009; ISSN 0273-2300.
23. Ghavami, K.; Toledo Filho, R.D.; Barbosa, N.P. Behaviour of composite soil reinforced with natural fibres. *Cem. Concr. Compos.* **1999**, *21*, 39–48. [[CrossRef](#)]
24. Mohammed, L.; Ansari, M.N.M.; Pua, G.; Jawaid, M.; Islam, M.S. A Review on Natural Fiber Reinforced Polymer Composite and Its Applications. *Int. J. Polym. Sci.* **2015**, *2015*, 1–15. [[CrossRef](#)]
25. Lopez, K.M.; Ravula, S.; Pérez, R.L.; Ayala, C.E.; Losso, J.N.; Janes, M.E.; Warner, I.M. Hyaluronic Acid–Cellulose Composites as Patches for Minimizing Bacterial Infections. *ACS Omega* **2020**, *5*, 4125–4132. [[CrossRef](#)]
26. Anton-Sales, I.; Beekmann, U.; Laromaine, A.; Roig, A.; Kralisch, D. Opportunities of Bacterial Cellulose to Treat Epithelial Tissues. *Curr. Drug Targets* **2019**, *20*, 808–822. [[CrossRef](#)]
27. Vargas-Rodríguez, L.; Arroyo Figueroa, G.; Herrera Méndez, C.H.; Pérez Nieto, A.; García Vieyra, M.I.; Rodríguez Núñez, J.R. Propiedades físicas del mucílago de nopal. *Acta Univ.* **2016**, *26*, 8–11. [[CrossRef](#)]
28. Espinosa-Andrews, H.; Urias-Silvas, J.E. Thermal properties of agave fructans (*Agave tequilana* Weber var. Azul). *Carbohydr. Polym.* **2012**, *87*, 2671–2676. [[CrossRef](#)]
29. Le Moigne, N.; Otazaghine, B.; Corn, S.; Angellier-Coussy, H.; Bergeret, A. *Surfaces and Interfaces in Natural Fibre Reinforced Composites*; Springer International Publishing: Cham, Switzerland, 2018. [[CrossRef](#)]
30. Skehan, P.; Storeng, R.; Scudiero, D.; Monks, A.; McMahon, J.; Vistica, D.; Warren, J.T.; Bokesch, H.; Kenney, S.; Boyd, M.R. New Colorimetric Cytotoxicity Assay for Anticancer-Drug Screening. *JNCI J. Natl. Cancer Inst.* **1990**, *82*, 1107–1112. [[CrossRef](#)] [[PubMed](#)]
31. Moya, L.; Zakeri, H.; Yamazaki, F.; Liu, W.; Mas, E.; Koshimura, S. 3D gray level co-occurrence matrix and its application to identifying collapsed buildings. *ISPRS J. Photogramm. Remote Sens.* **2019**, *149*, 14–28. [[CrossRef](#)]
32. Arzate Vazquez, I. Application of Image Texture Analysis for the Quantitative Characterization of Biological Surfaces. Ph.D. Thesis, Instituto Politecnico Nacional, México City, México, 2011.
33. Presutti, M. La matriz de co-ocurrencia en la clasificación multiespectral: Tutorial para la enseñanza de medidas texturales en cursos de grado universitario. In *4a Jornada de Educação Em Sensoriamento Remoto No Âmbito Do Mercosul*; Recursos Didáticos para o Ensino de Sensoriamento Remoto: São Leopoldo, Brasil, 2004; pp. 1–9.
34. Hall-Beyer, M. Practical guidelines for choosing GLCM textures to use in landscape classification tasks over a range of moderate spatial scales. *Int. J. Remote Sens.* **2017**, *38*, 1312–1338. [[CrossRef](#)]
35. Batchelor, B.; Waltz, F. *Intelligent Machine Vision—Techniques, Implementations and Applications*; Springer: London, UK, 2001; pp. 61–62.

36. Rodríguez, J.; Prieto, S.; Ortiz, L.; Wiesner, C.; Díaz, M.; Correa, C. Descripción matemática con dimensiones fractales de células normales y con anomalías citológicas de cuello uterino. *Rev. Cienc. Salud* **2006**, *4*, 58–63.
37. Jat, M.K.; Garg, P.K.; Khare, D. Monitoring and modelling of urban sprawl using remote sensing and GIS techniques. *Int. J. Appl. Earth Obs. Geoinf.* **2008**, *10*, 26–43. [[CrossRef](#)]
38. Chen, W.-S.; Yuan, S.-Y.; Hsieh, C.-M. Two algorithms to estimate fractal dimension of gray-level images. *Opt. Eng.* **2003**, *42*, 2452–2465. [[CrossRef](#)]
39. Rezwani, K.; Chen, Q.Z.; Blaker, J.J.; Boccaccini, A.R. Biodegradable and bioactive porous polymer/inorganic composite scaffolds for bone tissue engineering. *Biomaterials* **2006**, *27*, 3413–3431. [[CrossRef](#)]
40. Haralick, R.M.; Dinstein, I.; Shanmugam, K. Textural Features for Image Classification. *IEEE Trans. Syst. Man Cybern.* **1973**, *6*, 610–621. [[CrossRef](#)]
41. Korać, R.; Khambholja, K. Potential of herbs in skin protection from ultraviolet radiation. *Pharmacogn. Rev.* **2011**, *5*, 164. [[CrossRef](#)] [[PubMed](#)]
42. Domínguez-Fernández, R.N.; Arzate-Vázquez, I.; Chanona-Pérez, J.J.; Welti-Chanes, J.S.; Alvarado-González, J.S.; Calderon-Dominguez, G.; Garibay-Febles, V.; Gutierrez-Lopez, G.F. El gel de aloe vera: Estructura, composición química, procesamiento, actividad biológica e importancia en la industria farmacéutica y alimentaria. *Rev. Mex. Ing. Quim.* **2012**, *11*, 23–43.
43. Rivero, R.; Alustiza, F.; Capella, V.; Liaudat, C.; Rodríguez, N.; Bosch, P.; Barbero, C.; Rivarola, C. Physicochemical properties of ionic and non-ionic biocompatible hydrogels in water and cell culture conditions: Relation with type of morphologies of bovine fetal fibroblasts in contact with the surfaces. *Colloids Surf. B Biointerfaces* **2017**, *158*, 488–497. [[CrossRef](#)] [[PubMed](#)]
44. Howard, R.L.; Abotsi, E.; Jansen van, R.E.L.; Howard, S. Lignocellulose biotechnology: Issues of bioconversion and enzyme production. *Afr. J. Biotechnol.* **2003**, *2*, 602–619. [[CrossRef](#)]
45. Grolik, M.; Szczubiałka, K.; Wowra, B.; Dobrowolski, D.; Orzechowska-Wylegała, B.; Wylegała, E.; Nowakowska, M. Hydrogel membranes based on genipin-cross-linked chitosan blends for corneal epithelium tissue engineering. *J. Mater. Sci. Mater. Med.* **2012**, *23*, 1991–2000. [[CrossRef](#)]
46. Gao, L.; Gan, H.; Meng, Z.; Gu, R.; Wu, Z.; Zhang, L.; Zhu, X.; Sun, W.; Li, J.; Zheng, Y.; et al. Effects of genipin cross-linking of chitosan hydrogels on cellular adhesion and viability. *Colloids Surf. B Biointerfaces* **2014**, *117*, 398–405. [[CrossRef](#)] [[PubMed](#)]
47. Gürbay, A.; Gonthier, B.; Barret, L.; Favier, A.; Hincal, F. Cytotoxic effect of ciprofloxacin in primary culture of rat astrocytes and protection by Vitamin E. *Toxicology* **2007**, *229*, 54–61. [[CrossRef](#)]
48. Cisneros-López, E.O.; Anzaldo, J.; Fuentes-Talavera, F.J.; González-Núñez, R.; Robledo-Ortiz, J.R.; Rodrigue, D. Effect of agave fiber surface treatment on the properties of polyethylene composites produced by dry-blending and compression molding. *Polym. Compos.* **2017**, *38*, 96–104. [[CrossRef](#)]
49. Cacicedo, M.L.; Islan, G.A.; Drachemberg, M.F.; Alvarez, V.A.; Bartel, L.C.; Bolzán, A.C.; Castro, G.R. Hybrid bacterial cellulose-pectin films for delivery of bioactive molecules. *RSC New J. Chem.* **2018**, *42*, 7457–7467. [[CrossRef](#)]
50. Sampath, U.; Ching, Y.; Chuah, C.; Sabariah, J.; Lin, P.-C. Fabrication of Porous Materials from Natural/Synthetic Biopolymers and Their Composites. *Materials* **2016**, *9*, 991. [[CrossRef](#)]
51. Miao, X.; Sun, D. Graded/Gradient Porous Biomaterials. *Materials* **2009**, *3*, 26–47. [[CrossRef](#)]
52. Gavillon, R.; Budtova, T. Aerocellulose: New Highly Porous Cellulose Prepared from Cellulose–NaOH Aqueous Solutions. *Biomacromolecules* **2008**, *9*, 269–277. [[CrossRef](#)] [[PubMed](#)]
53. Capitani, D.; Crescenzi, V.; De Angelis, A.A.; Segre, A.L. Water in Hydrogels. An NMR Study of Water/Polymer Interactions in Weakly Cross-Linked Chitosan Networks. *Macromolecules* **2001**, *34*, 4136–4144. [[CrossRef](#)]
54. Migneault, I.; Dartiguenave, C.; Bertrand, M.J.; Waldron, K.C. Glutaraldehyde: Behavior in Aqueous Solution, Reaction with Proteins, and Application to Enzyme Crosslinking. *BioTechniques* **2004**, *37*, 790–802. [[CrossRef](#)]
55. Pereira, P.H.F.; Oliveira, T.Í.S.; Rosa, M.F.; Cavalcante, F.L.; Moates, G.K.; Wellner, N.; Waldron, K.W.; Azeredo, H.M. Pectin extraction from pomegranate peels with citric acid. *Int. J. Biol. Macromol.* **2016**, *88*, 373–379. [[CrossRef](#)] [[PubMed](#)]
56. Madera-Santana, T.J.; Vargas-Rodríguez, L.; Núñez-Colín, C.A.; González-García, G.; Peña-Caballero, V.; Núñez-Gastélum, J.A.; Gallegos-Vázquez, C.; Rodríguez-Núñez, J.R. Mucilage from cladodes of *Opuntia spinulifera* Salm-Dyck: Chemical, morphological, structural and thermal characterization. *CyTA—J. Food* **2018**, *16*, 650–657. [[CrossRef](#)]

57. Femenia, A.; García-Pascual, P.; Simal, S.; Rosselló, C. Effects of heat treatment and dehydration on bioactive polysaccharide acemannan and cell wall polymers from *Aloe barbadensis* Miller. *Carbohydr. Polym.* **2003**, *51*, 397–405. [[CrossRef](#)]
58. Camelo Caballero, L.R.; Wilches-Torres, A.; Cárdenas-Chaparro, A.; Gómez Castaño, J.A.; Otálora, M.C. Preparation and Physicochemical Characterization of Softgels Cross-Linked with Cactus Mucilage Extracted from Cladodes of *Opuntia Ficus-Indica*. *Molecules* **2019**, *24*, 2531. [[CrossRef](#)]
59. Nizama, F.; Borja, N.; Rocha, G.; Infante, A.; Teixeira, B.; Casalino, A. Análisis por espectroscopía UV y FTIR de macerados acuosos y alcohólicos de *Aloe vera* L. y *Aloe barbadensis* Miller. Interacción con sales inorgánicas. *Rev. Soc. Química Perú* **2010**, *76*, 242–260.
60. Muthukumar, P.; Divya, R.; Indhumathi, E.; Keerthika, C. Total phenolic and flavonoid content of membrane processed *Aloe vera* extract: A comparative study. *Int. Food Res. J.* **2018**, *25*, 1450–1456.
61. Ray, A.; Ghosh, S. Chemometrics for Functional Group Distribution, and UV Absorption Potential of *Aloe vera* L. Gel at Different Growth Periods. *Mater. Today Proc.* **2018**, *5*, 22245–22253. [[CrossRef](#)]
62. Duhoranimana, E.; Karangwa, E.; Lai, L.; Xu, X.; Yu, J.; Xia, S.; Zhang, X.; Muhoza, B.; Habinshuti, I. Effect of sodium carboxymethyl cellulose on complex coacervates formation with gelatin: Coacervates characterization stabilization and formation mechanism. *Food Hydrocoll.* **2017**, *69*, 111–120. [[CrossRef](#)]
63. Kumar, M.S.; Datta, P.K.; Dutta Gupta, S. In vitro evaluation of UV opacity potential of *Aloe vera* L. gel from different germplasms. *J. Nat. Med.* **2009**, *63*, 195–199. [[CrossRef](#)] [[PubMed](#)]
64. Landry, L.G.; Chapple, C.; Last, R.L. Arabidopsis Mutants Lacking Phenolic Sunscreens Exhibit Enhanced Ultraviolet-B Injury and Oxidative Damage. *Plant Physiol.* **1995**, *109*, 1159–1166. [[CrossRef](#)] [[PubMed](#)]
65. Maddocks-Jennings, W.; Wilkinson, J.M.; Shillington, D. Novel approaches to radiotherapy-induced skin reactions: A literature review. *Complement. Ther. Clin. Pract.* **2005**, *11*, 224–231. [[CrossRef](#)] [[PubMed](#)]
66. Rabe, J.H.; Mamelak, A.J.; McElgunn, P.J.S.; Morison, W.L.; Sauder, D.N. Photoaging: Mechanisms and repair. *J. Am. Acad. Dermatol.* **2006**, *55*, 1–19. [[CrossRef](#)] [[PubMed](#)]
67. Marionnet, C.; Tricaud, C.; Bernerd, F. Exposure to non-extreme solar UV daylight: Spectral characterization, effects on skin and photoprotection. *Int. J. Mol. Sci.* **2014**, *16*, 68–90. [[CrossRef](#)]
68. Sadeghifar, H.; Venditti, R.; Jur, J.; Gorga, R.E.; Pawlak, J.J. Cellulose-Lignin Biodegradable and Flexible UV Protection Film. *ACS Sustain. Chem. Eng.* **2017**, *5*, 625–631. [[CrossRef](#)]
69. Teacă, C.-A.; Roşu, D.; Bodîrlău, R.; Roşu, L. Structural changes in wood under artificial UV light irradiation determined by FTIR spectroscopy and color measurements—A brief review. *BioResources* **2013**, *8*, 1478–1507. [[CrossRef](#)]
70. Villalobos, R.; Chanona, J.; Hernández, P.; Gutiérrez, G.; Chiralt, A. Gloss and transparency of hydroxypropyl methylcellulose films containing surfactants as affected by their microstructure. *Food Hydrocoll.* **2005**, *19*, 53–61. [[CrossRef](#)]

